Canadian Mineralogist
Vol. 22, pp. 401-409 (1984)

FAYALITE AND CLINOPYROXENE IN THE PORPHYRIES OF THE TIBCHI ANOROGENIC RING-COMPLEX, NIGERIA: POSTMAGMATIC INITIATION OF A PERALKALINE TREND

ECHEFU C. IKE
Department of Geology, Ahmadu Bello University, Zaria, Nigeria

PETER BOWDEN
Department of Geology, University of St. Andrews, St. Andrews, Fife, Scotland KY16 9ST

ROBERT F. MARTIN
Department of Geological Sciences, McGill University, 3450 University Street, Montreal, Quebec H3A 2A7

ABSTRACT

The quartz and granite porphyries of the Tibchi anorogenic ring-complex, Nigeria, and their monzonitic and syenitic enclaves, contain fayalite and a clinopyroxene whose composition varies from ferroaugite to ferrohedenbergite to sodian hedenbergite. The fayalite, which is unzoned, ranges from Fa_{92} to Fa_{99} in composition; this spread allows the ranking of the quartz porphyry and its enclaves in a crystallization sequence. The Fe content of pyroxene grains increases outward; the most evolved magmatic composition crystallized as hedenbergite rather than as β-wollastonite. The proportion of the Ac component, which is low during most of the crystallization interval, increases markedly at a late stage; the formation of the rim is attributed to a residual fluid phase that could penetrate along cleavage planes. Residence time of this pore fluid probably was longer in the granite porphyry; the magma rose quietly along a ring fault after the evacuation of the magmatic reservoir by fluidization. Compared to the quartz porphyry that resulted from this rapid emplacement, the granite porphyry contains no fayalite and shows a more thorough reaction between early-formed magmatic pyroxene and the fluid phase. At Tibchi, the appearance of a peralkaline overprint occurred at the postmagmatic stage.

Keywords: quartz porphyry, granite porphyry, fayalite, hedenbergite, acmite, peralkalinity, postmagmatic stage, Tibchi, Nigeria, ring complex, anorogenic.

SOMMAIRE

Le porphyre à phenocristaux de quartz et le porphyre granitique du complexe annulaire anorogénique de Tibchi (Nigéria), ainsi que leurs enclaves monzonitique et syénitique, contiennent de la fayalite et un clinopyroxène dont la composition va de ferroaugite à ferrohédenbergite à hédenbergite sodique. La fayalite, qui est non-zonée, a une composition comprise entre Fa_{92} et Fa_{99}; ce domaine de composition permet d'ordonner les échantillons de porphyre à quartz et les enclaves dans une séquence de cristallisation. Le pyroxène montre un enrichissement en fer vers la bordure; la composition magmatique la plus évoluée a cristallisé sous forme de hédenbergite plutôt que de wollastonite-β. La proportion du terme Ac, qui demeure faible pendant la majeure partie de l'intervalle de cristallisation, augmente de façon frappante à un stade tardif; on attribue la formation de la surcroissance enrichie en Ac à une phase fluide capable de s'infiltrer le long des clivages. La durée de l'interaction avec cette phase fluide interstitielle a été la plus longue dans le cas du porphyre granitique. Le magma a été mis en place tranquillement le long d'une faille annulaire après évacuation de la partie supérieure de la chambre magmatique par fluidisation. Comparée au porphyre à phénocristaux de quartz, qui a résulté de cette mise en place soudaine, le porphyre granitique ne contient aucune trace de fayalite et montre une réaction plus poussée entre les compositions magmatiques de pyroxène, formées d'abord, et la phase fluide résiduelle. A Tibchi, le caractère hyperalcalin s'est manifesté au stade post-magmatique de cristallisation.

Mots-clés: porphyre à quartz, porphyre granitique, fayalite, hédenbergite, acmite, hyperalcalinité, stade post-magmatique, Tibchi (Nigéria), complexe annulaire, anorogénique.

INTRODUCTION

The Tibchi ring-complex forms part of the well-known belt of high-level anorogenic intrusive bodies that collectively define the Younger Granite province of Nigeria and Niger. The emplacement of these epizonal complexes, and of analogues in eastern Canada and the United States, signals the inception of rifting culminating in the opening of the Atlantic Ocean. The Tibchi ring-complex, which is Late Jurassic (a Rb–Sr isochron gives 175 ± 3 Ma: M. A. Rahaman, pers. comm. 1977), consists mainly of rocks of granitic composition; in the Younger Granite province as a whole, such rocks constitute more than 90% of the igneous rocks exposed. The reader will find descriptions of the various ring-complexes in Jacobson *et al.* (1958), Buchanan *et al.* (1971), Bowden & Turner (1974), Turner (1976), Turner & Bowden (1979), Martin & Bowden (1981) and Bowden (1982). Whereas many of these complexes are well mapped, only now are quantitative mineralogical data becoming available. Here, we focus on the microphenocrystic mafic minerals of the Tibchi granitic porphyries and their genetically related enclaves.

Past investigators of the ferromagnesian minerals in these anorogenic rocks [Bain (1934) on fayalite

from Kudaru, Borley (1963) on ferroaugite from Pankshin, Jacobson *et al.* (1958) on fayalite and hedenbergite from Ririwai] were hampered by the textural complexity of the multiphase clusters. The only valid tool in studies of this type is the electron microprobe. This overcomes the problems posed by the small modal proportion of the mafic minerals in these rocks (between 0.5 and 2% by volume) and the intergrown Fe–Ti oxide minerals.

Description of the Complex

The Tibchi complex consists of an annular dyke of granite porphyry, a central mass dominated by biotite granite, a plug of quartz porphyry and a suite of related ignimbritic rocks (Fig. 1). The narrow ring-dyke was formed after cauldron subsidence and partial evacuation through fluidization of the subvolcanic reservoir (Ike 1983). The complex covers approximately 16 × 27 km; most of its area, at the present level of erosion, is occupied by the basement metamorphic complex, mainly consisting of gneissic granite of Pan-African age.

Directly relevant to this mineralogical study is a suite of enclaves that are encountered in the porphyritic units. These enclaves are closely

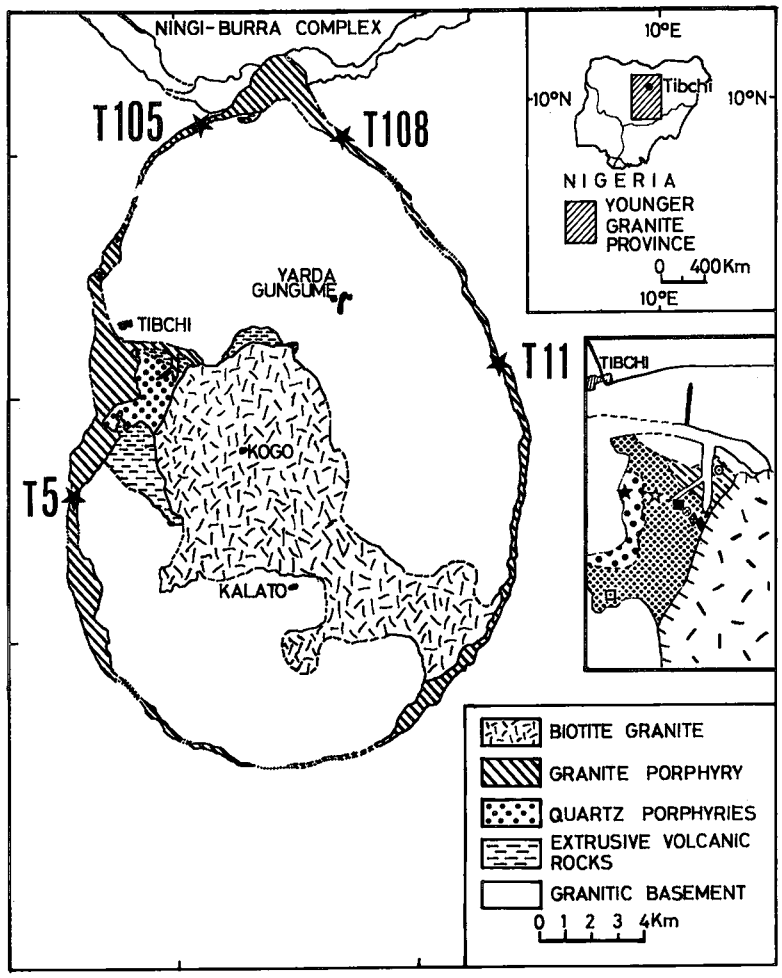

FIG. 1. Simplified geological map of the Tibchi complex, showing the major rock-units. The ring dyke of granite porphyry overlaps the southernmost portion of the Ningi–Burra complex. The basement complex consists mainly of gneissic granite emplaced during the Pan-African orogeny. The complex was mapped by E.C. Ike. Middle inset is a detailed sketch of the area south and east of the village of Tibchi, showing the following sample locations: black star T60, white star T135, black square T167, white square T115, black diamond T170, white diamond T169, dotted circle T133, crossed circle T168. Width of middle inset represents 3.3 km.

interrelated petrographically; also, they are considered cognate with respect to the host porphyries. The contact between host and enclave typically is diffuse and irregular. Two lithologies are found as enclaves: monzonite and syenite. These more basic rocks may have formed from melts that were precursors of those that gave the porphyries.

In the Tibchi complex, fayalite is restricted to the quartz porphyry and to enclaves of monzonite. Clinopyroxene, which belongs to the series ferroaugite – ferrohedenbergite, occurs in quartz porphyry, in the granite porphyry ring-dyke, and in the enclaves.

The quartz porphyry

The pristine samples of quartz porphyry (Fig. 2) are dark green; the phenocrysts of quartz (paramorphic after β-quartz), clear green alkali feldspar (originally sanidine, now orthoclase perthite), ferrohedenbergitic clinopyroxene and fayalite, which commonly are fragmented, account for 40 to 50% of the rock by volume. The unit of quartz porphyry grades into crystal-rich ignimbrites, and represents a frozen feeder to the latter (Ike 1983). Xenoliths of earlier ignimbrite and related felsic intrusive rocks are common in addition to the cognate plutonic enclaves already mentioned.

Based principally on the nature of the clinopyroxene, two variants of the quartz porphyry may be recognized: 1) a fayalite – ferroaugite – ferrohedenbergite type, and 2) a fayalite – ferrohedenbergite type. In type 1, the clinopyroxene varies continuously from ferroaugite to ferrohedenbergite. Pleochroism increases from the ferroaugite core to the sodian ferrohedenbergite rim; the rim has a larger extinction angle ($\gamma \wedge c \simeq 50°$) than the core by up to 5°. The ferroaugite core, although prismatic, commonly displays a skeletal outline, indicative of a larger degree of supercooling during early crystallization. The microcrystalline groundmass appears to contain ferrohedenbergite only.

In the more fractionated, ferroaugite-free variety of quartz porphyry (*e.g.*, Fig. 3A, B, specimen T105), zoning in the ferrohedenbergite microphenocrysts is more prominent: a yellowish core of ferrohedenbergite gives way to a bright green rim of sodian hedenbergite. This rim can be followed along cracks and cleavage planes into the ferrohedenbergite core of the phenocryst. The prisms commonly show roundish tips and an irregular outline, perhaps indicative of a limited degree of supercooling.

Fayalite microphenocrysts account for 0.5% (vol.) of the quartz porphyry. The pale yellow, equidimensional and anhedral grains are heavily fractured and partly altered. Birefringence is strong

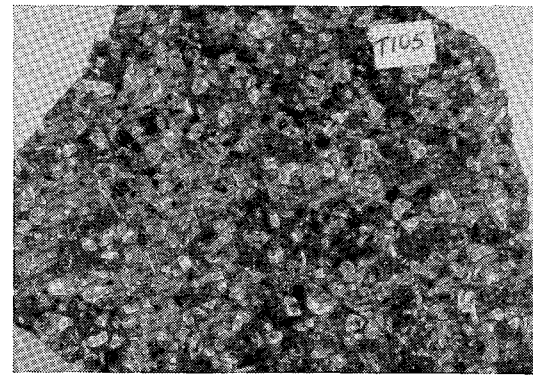

FIG. 2. Typical specimen of quartz porphyry from Tibchi. Note the fragmental appearance of the phenocrysts, an ignimbritic tendency. Specimen T105. Width of label 1 cm.

with respect to ferrohedenbergite, which commonly forms a rim of small anhedral to subhedral crystals.

The microcrystalline groundmass locally displays striking devitrification textures, mainly spherulites in various stages of coarsening. It consists of alkali feldspar (typically a mixture of orthoclase + intermediate microcline + albite), quartz, ferrohedenbergite, ferrian ilmenite (Ike & Bowden, in press), monazite, apatite, zircon and fluorite. The opaque mineral occluded in the microphenocrysts of pyroxene and fayalite (Figs. 3A, B) is ilmenite (Ike & Bowden, in press). Aenigmatite was sought but not found.

Representative bulk compositions of quartz porphyry are listed in Table 1.

The granite porphyry

The rock that occupies the ring-dyke fracture (Fig. 1) is coarsely porphyritic (Fig. 4) and greyish green where fresh. There is a general tendency for this color to change to brown within hours on a fresh surface of a specimen, reflecting the rapid oxidation of exposed grains. The dominant phenocrysts, which make up about 40% by volume, consist of turbid perthitic alkali feldspar (typically intermediate microcline + albite), quartz and clinopyroxene. The alkali feldspar phenocrysts may show synneusis, giving the rock a glomeroporphyritic texture. The ferroaugite – ferrohedenbergite microphenocrysts are more obviously zoned than in the quartz porphyry. Pale brown ferroaugite is transitional to pale greenish brown ferrohedenbergite. In some specimens, the ferrohedenbergite grades into a rim of bright green sodian hedenbergite. The groundmass is relatively coarse, and microgranitic to micrographic.

Representative bulk-compositions of granite porphyry are listed in Table 1.

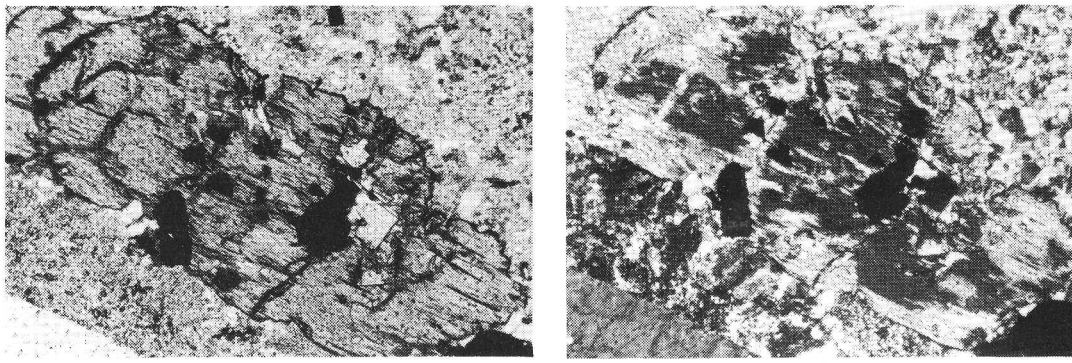

FIG. 3. A. Phenocryst of ferrohedenbergite – sodian hedenbergite set in a microcrystalline groundmass of alkali feldspar, quartz and Fe-rich clinopyroxene. Specimen T105. Width of field of view 2 mm, plane-polarized light. B. Same crystal, in crossed-polarized light. The zonation of the crystal is brought out by a difference in extinction angle between ferrohedenbergite (core, yellowish in plane light) and sodian hedenbergite (rim, bright green in plane light). Note that the sodian hedenbergite zone follows cracks and cleavage planes as it encroaches on the core.

TABLE 1. REPRESENTATIVE BULK-COMPOSITIONS OF QUARTZ PORPHYRY AND GRANITE PORPHYRY, TIBCHI RING-COMPLEX

		T60	T105	T11	T108	T5
SiO_2	wt. %	73.50	73.00	72.75	72.98	72.98
TiO_2		0.30	0.37	0.35	0.30	0.30
Al_2O_3		11.38	12.68	12.54	11.38	11.42
Fe_2O_3		1.46	1.43	2.22	2.82	2.07
FeO		2.35	1.98	1.46	0.98	1.78
MnO		0.08	0.08	0.06	0.08	0.11
MgO		0.08	0.08	0.09	0.12	0.08
CaO		1.04	0.93	0.81	0.83	0.83
Na_2O		4.30	4.01	4.09	4.07	4.19
K_2O		5.06	5.10	5.21	5.10	5.08
P_2O_5		0.03	0.00	0.04	0.03	0.03
H_2O^+		0.24	0.36	0.61	0.75	0.54
H_2O^-		0.12	0.11	0.11	0.23	0.04
Total		99.94	100.13	100.34	99.67	99.45
A.I.		1.10	0.96	0.98	1.07	1.09
D.I.		88.20	91.87	93.19	89.94	88.68

Specimens: T60, T105 quartz porphyry, T11, T108, T5 granite porphyry, sampled from the ring dyke. A.I. agpaitic index, D.I. differentiation index. Analysts: R.A. Batchelor and E.C. Ike. Analyses by atomic absorption.

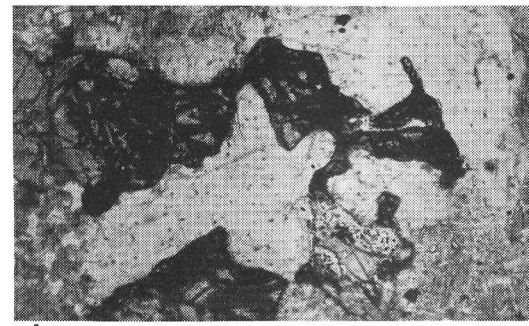

FIG. 5. Mineral assemblage in a typical monzonitic enclave, this one found in T105, a specimen of quartz porphyry. Fayalite crystals (dark) appear interstitial relative to earlier-formed plagioclase (light). Note the abundance of apatite needles. Width of field of view 1 mm, crossed-polarized light.

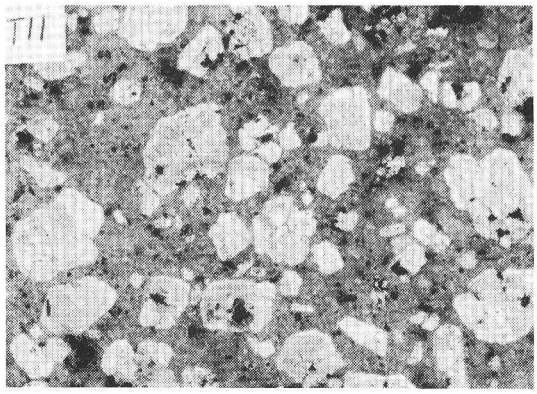

FIG. 4. Typical specimen of granite porphyry from Tibchi. Note the conspicuous synneusis involving the feldspar phenocrysts, which gives the rock a distinctly glomeroporphyritic texture. Specimen T11. Width of label 1 cm.

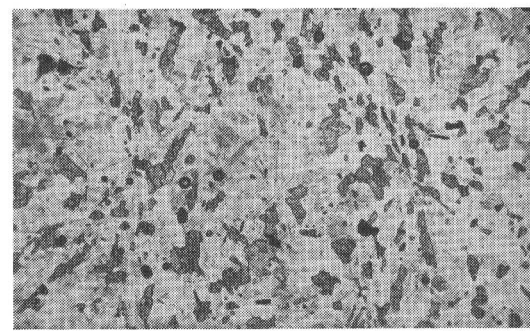

FIG. 6. Mineral assemblage and textural development in a typical microsyenite enclave, this one found in granite porphyry specimen T11. Note the skeletal appearance of the ferrohedenbergite crystals, which nucleated along rays in a spherulitic intergrowth. Width of field of view 2 mm, plane-polarized light.

Monzonite enclaves

The enclaves of fine-grained monzonite contain fayalite, ferroaugite, sodic andesine (An_{32}, Michel-Lévy method) apatite and ilmenite (Ike & Bowden, in press). The fayalite and ferroaugite form interstitial clusters between plagioclase grains (Fig. 5) that generally show a striking rim of homogeneous, turbid K-feldspar. Discrete grains of K-feldspar are absent. Apatite needles define a criss-cross arrangement in the plagioclase (Fig. 5); ilmenite is sparse and enclosed in the mafic minerals.

Microsyenite enclaves

The cognate xenoliths of microsyenite contain alkali feldspar, oligoclase, ferrohedenbergite, titanomagnetite (Ike & Bowden, in press), apatite and accessory quartz. One variant is characterized by lath-shaped feldspar grains and anhedral grains of clinopyroxene that define a crude spherulitic array (Fig. 6). In another variant, the same minerals define a subparallel arrangement; in a third, which is essentially equigranular, the clinopyroxene clearly is interstitial to feldspar. Hints of a porphyritic texture have also been found in some quartz-bearing microsyenitic enclaves.

In contrast to the monzonite enclaves, the K-feldspar here does occur as a discrete phase as well as a rim around the plagioclase. The proportion of the two feldspars varies widely, and the group name 'syenite' is used here mainly for convenience.

Analytical Data on the Mafic Minerals

The olivine and clinopyroxene have been analyzed by electron microprobe (Cambridge Microscan V located at the University of Edinburgh). The microprobe was operated in the wavelength-dispersion mode at 20 kV and 30 nA, with a beam-spot size of 1 μm. The following standards were used: wollastonite (Ca, Si), rutile (Ti), corundum (Al), purified metals (Fe, Mn), periclase (Mg), jadeite and halite (Na) and orthoclase (K). Data were reduced by full ZAF correction, as described by Sweatman & Long (1969). Total iron, originally expressed as FeO, has been recalculated to give FeO and Fe_2O_3 using the method of Finger (1972), in which the amount of ferric iron is constrained by the number of cations and oxygen atoms in the structural formula. Individual grains of fayalite show no significant compositional zonation, nor is there significant variation from one grain to the next. For each specimen examined, the composition quoted (Table 2) represents an average of many determinations. The representative data for ferroaugite (Table 3) and ferrohedenbergite (Table 4) are presented separately for convenience, in spite of continuous zonation recorded in individual crystals.

Mineral Compositions

Fayalite

The olivine in the four Tibchi specimens selected for study ranges in composition from Fa_{92} to Fa_{99} (Table 2, Fig. 7). The composition of the olivine can

TABLE 2. COMPOSITION OF OLIVINE FROM THE TIBCHI COMPLEX

	1	2	3	4
SiO_2 wt.%	30.39	29.85	29.41	29.59
TiO_2	0.03	0.05	0.00	0.03
Al_2O_3	0.03	0.04	0.06	0.03
Fe_2O_3	0.00	0.00	0.34	0.00
FeO	64.26	66.71	66.33	67.38
MnO	1.74	1.99	1.77	1.81
MgO	3.23	1.05	1.07	0.28
CaO	0.36	0.38	0.39	0.32
total	100.04	100.07	99.37	99.44
	Number of ions on the basis of 3 cations			
Si	1.003	1.002	0.994	1.005
^{iv}Al	-	-	0.002	-
^{vi}Al	0.001	0.002	-	0.001
Ti	0.001	0.001	-	0.001
Fe^{3+}	-	-	0.009	-
Fe^{2+}	1.774	1.872	1.876	1.915
Mn	0.049	0.057	0.051	0.052
Mg	0.159	0.052	0.054	0.014
Ca	0.013	0.014	0.014	0.012
Fa	91.99	97.34	97.45	99.28

Compositions were determined by electron-microprobe analysis. The ratio 100(Fe+Mn)/(Fe+Mn+Mg) gives Fa, the mole % fayalite component. Specimens studied: 1. fine-grained monzonite enclave in quartz porphyry; 2. quartz porphyry T60; 3. quartz porphyry T105; 4. quartz porphyry T115.

TABLE 3. COMPOSITION OF FERROAUGITE FROM THE TIBCHI COMPLEX, NIGERIA

	1	2	3	4	5	6	7	8
SiO_2 wt.%	49.12	49.18	48.68	49.30	49.06	49.34	49.05	48.41
TiO_2	0.62	0.60	0.70	0.08	0.03	0.34	0.31	0.34
Al_2O_3	1.22	1.21	1.57	1.32	0.52	0.51	0.51	0.45
Fe_2O_3	1.30	1.77	3.22	0.72	0.68	1.48	2.51	1.78
FeO	21.75	21.64	20.12	22.24	25.64	23.55	24.05	25.46
MnO	0.59	0.56	0.67	0.66	0.68	0.65	0.76	0.77
MgO	6.36	5.99	5.91	6.62	3.71	4.79	4.28	3.31
CaO	18.66	18.99	18.38	17.86	18.73	19.12	19.10	18.76
Na_2O	0.38	0.47	0.84	0.46	0.39	0.44	0.44	0.45
K_2O	x	x	x	x	x	0.01	x	x
total	100.00	100.41	100.09	99.26	99.44	100.23	101.01	99.73
FeO(T)	22.92	23.24	23.02	22.88	26.26	24.89	26.31	27.06
	Number of ions on the basis of 4 cations							
Si	1.948	1.946	1.928	1.963	1.991	1.973	1.958	1.969
^{iv}Al	0.052	0.054	0.072	0.037	0.009	0.024	0.024	0.022
^{vi}Al	0.005	0.002	0.001	0.025	0.016	-	-	-
Ti	0.019	0.018	0.021	0.003	0.001	0.010	0.009	0.010
Fe^{3+}	0.039	0.053	0.096	0.022	0.021	0.045	0.075	0.054
Fe^{2+}	0.721	0.716	0.666	0.740	0.870	0.787	0.803	0.866
Mn	0.020	0.019	0.022	0.022	0.023	0.022	0.026	0.026
Mg	0.376	0.353	0.349	0.392	0.224	0.285	0.254	0.201
Ca	0.792	0.805	0.780	0.761	0.814	0.819	0.816	0.817
Na	0.029	0.036	0.065	0.036	0.031	0.034	0.034	0.035
K	-	-	-	-	-	-	-	-
Ca at.%	40.66	41.37	40.89	39.29	41.70	41.83	41.34	41.60
Fe	40.04	40.49	42.43	40.47	46.82	43.61	45.79	48.17
Mg	19.30	18.14	16.68	20.24	11.48	14.56	12.87	10.23

FeO(T): total iron expressed as FeO. Compositions were determined by electron-microprobe analysis. x less than 0.004% or absent. In calculating Fe (at.%), Fe^{3+} + Fe^{2+} + Mn was considered equal to Fe. The host rocks: 1, 2, 3 fine-grained monzodiorite enclave in quartz porphyry; 4, 5 granite porphyry (from ring-dyke) T11; 4 represents the core of an extensively zoned phenocryst whose rim composition is given in column 18, Table 3; 6, 7, 8 zoned skeletal (quenched) ferroaugite phenocryst in quartz porphyry T60.

TABLE 4. COMPOSITION OF FERROHEDENBERGITE FROM THE TIBCHI COMPLEX, NIGERIA

		1	2	3	4	5	6	7	8	9	10	11	12	13	14	15	16	17	18	19	20
SiO_2	wt.%	48.18	49.69	48.51	47.52	47.74	48.40	46.81	47.95	48.37	47.36	47.80	48.68	47.67	47.82	48.49	47.95	48.78	48.72	47.46	48.64
TiO_2		0.69	x	0.33	0.74	0.70	0.32	0.79	0.40	0.17	0.05	0.02	0.25	0.39	0.30	0.29	0.23	0.26	x	0.08	x
Al_2O_3		1.57	0.11	0.43	0.93	0.90	0.45	0.68	0.29	0.27	0.93	0.40	0.20	0.49	0.30	0.23	0.23	0.54	0.22	0.90	0.19
Fe_2O_3		3.02	0.58	1.20	1.90	0.84	1.07	2.23	1.10	2.16	2.96	2.57	5.34	0.92	1.77	2.87	0.95	2.66	4.71	1.93	2.43
FeO		24.72	27.01	28.69	25.69	28.23	28.73	28.86	28.92	26.02	26.92	27.61	24.60	29.77	29.34	27.95	30.08	27.52	23.91	28.32	26.51
MnO		0.76	0.71	0.74	0.89	0.82	0.76	0.89	0.78	0.80	0.91	0.82	0.79	0.76	0.76	0.76	0.65	0.80	0.74	0.78	0.79
MgO		3.12	2.68	1.70	2.64	1.78	1.37	0.62	1.27	2.34	1.45	1.43	0.96	1.12	0.32	0.40	0.13	0.18	1.74	0.92	1.34
CaO		18.02	19.06	18.77	19.39	18.63	18.62	18.60	18.59	19.68	19.09	18.71	17.09	17.36	18.87	17.66	18.82	15.44	18.64	18.97	19.36
Na_2O		0.88	0.55	0.39	0.29	0.36	0.51	0.43	0.42	0.38	0.39	0.39	2.04	0.43	0.57	1.34	0.54	2.19	1.43	0.39	0.79
K_2O		x	x	x	0.01	x	0.01	x	x	x	x	x	x	0.19	x	x	x	x	x	x	x
total		100.92	100.39	100.76	100.00	100.00	100.24	99.91	99.72	100.19	100.06	99.75	99.95	99.10	100.05	99.99	99.58	98.37	100.11	99.75	100.05
FeO(T)		27.44	27.53	29.77	27.39	28.99	29.68	30.86	29.91	27.97	29.59	30.01	29.41	30.59	30.94	30.53	30.94	29.91	28.15	30.06	28.70
		Number of ions on the basis of 4 cations																			
Si		1.931	2.010	1.977	1.938	1.958	1.984	1.941	1.980	1.971	1.946	1.970	1.986	1.984	1.979	1.994	1.994	2.025	1.979	1.961	1.990
^{IV}Al		0.069	-	0.021	0.045	0.043	0.016	0.033	0.014	0.013	0.045	0.019	0.010	0.016	0.015	0.006	0.006	-	0.011	0.039	0.009
^{VI}Al		0.005	0.005	-	-	-	0.006	-	-	-	-	-	-	0.008	-	0.006	0.005	0.026	-	0.005	-
Ti		0.021	-	0.010	0.023	0.022	0.010	0.025	0.012	0.005	0.002	0.001	0.008	0.012	0.010	0.009	0.007	0.008	-	0.003	-
Fe^{3+}		0.091	0.018	0.037	0.058	0.026	0.033	0.069	0.034	0.066	0.092	0.080	0.164	0.029	0.055	0.089	0.030	0.083	0.144	0.060	0.075
Fe^{2+}		0.829	0.913	0.977	0.876	0.968	0.984	1.001	0.999	0.886	0.925	0.957	0.839	1.036	1.015	0.961	1.046	0.955	0.812	0.978	0.907
Mn		0.026	0.024	0.025	0.031	0.028	0.026	0.031	0.027	0.027	0.032	0.028	0.027	0.027	0.027	0.026	0.023	0.028	0.025	0.027	0.027
Mg		0.187	0.161	0.103	0.161	0.109	0.083	0.039	0.078	0.142	0.089	0.088	0.058	0.070	0.020	0.025	0.008	0.011	0.105	0.056	0.081
Ca		0.774	0.826	0.819	0.847	0.818	0.817	0.826	0.822	0.859	0.840	0.826	0.747	0.774	0.836	0.778	0.838	0.687	0.811	0.839	0.848
Na		0.068	0.043	0.031	0.023	0.028	0.041	0.035	0.034	0.030	0.031	0.032	0.162	0.035	0.045	0.107	0.044	0.176	0.113	0.031	0.063
K		-	-	-	-	-	0.001	-	-	-	-	-	-	0.010	-	-	-	-	-	-	-
Ca	at.%	40.59	42.53	41.76	42.93	41.97	42.04	42.02	41.94	43.38	42.47	41.74	40.71	39.98	42.81	41.41	43.08	38.92	42.75	42.81	43.76
Fe		49.61	49.18	52.98	49.91	52.44	53.68	56.00	54.08	49.45	53.03	53.81	56.13	56.40	56.17	57.26	56.51	60.43	51.71	54.33	52.06
Mg		9.80	8.29	5.26	8.16	5.59	4.28	1.98	3.98	7.17	4.50	4.45	3.16	3.62	1.02	1.33	0.41	0.65	5.54	2.86	4.18

FeO(T): total iron expressed as FeO. Compositions were determined by electron-microprobe analysis. x less than 0.004% or absent. In calculating Fe (at.%), Fe^{3+} + Fe^{2+} + Mn was considered equal to Fe. The host rocks: 1 fine-grained monzodiorite enclave in quartz porphyry; 2, 3 microsyenite enclave in quartz porphyry; 4 → 7 phenocrysts in quartz porphyry T60; 8 phenocryst in quartz porphyry T169; 9 phenocryst in quartz porphyry T168; 10, 11 core and rim of phenocryst, quartz porphyry T105; 12 sodian ferrohedenbergite core, 13 ferrohedenbergite rim, quartz porphyry T135, 14, 15 zoned phenocryst, quartz porphyry T115; 16, 17 ferrohedenbergite core and sodian ferrohedenbergite rim, quartz porphyry T115; 18 rim on ferroaugite (column 4, Table 2), granite porphyry T11; 19, 20 rim and core of phenocryst, granite porphyry (ring dyke) T11.

be used as an index of evolution, to rank the specimens in the following order of increasing degree of iron enrichment: 1) fayalite – ferroaugite micromonzodiorite enclave (Fa_{92}), 2) fayalite – ferroaugite – ferrohedenbergite quartz porphyry T60 ($Fa_{97.3}$), 3) fayalite – ferrohedenbergite quartz porphyry T105 and T115 ($Fa_{97.5}$, $Fa_{99.3}$). The Mn content of olivine remains approximately constant in this series, which suggests that the enclave does form part of the suite. Note that the compositions inferred (Table 2) may differ significantly from reality, in view of new findings that "fayalite" may

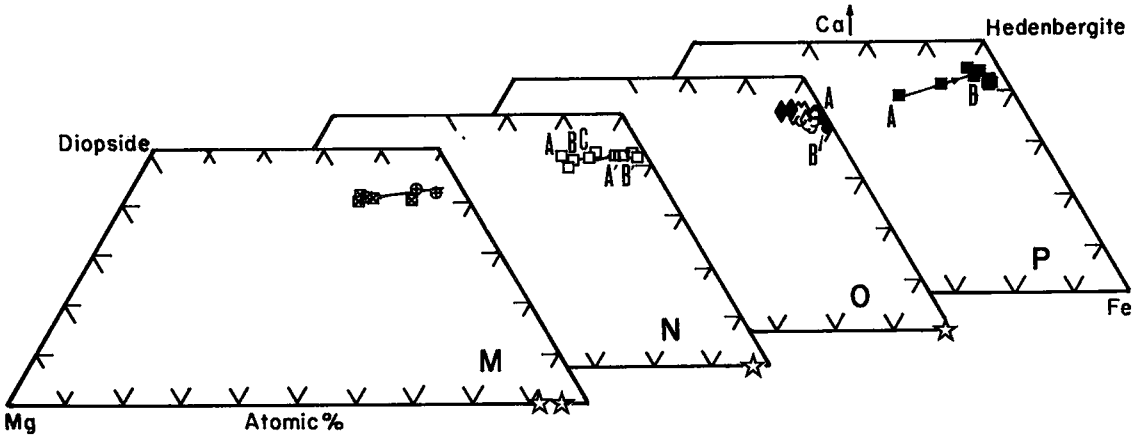

FIG. 7. Trends of crystallization for clinopyroxene in the Tibchi complex. Compositions are plotted separately for the enclaves (M), quartz porphyry (N, O) and granite porphyry (P). Also shown is the composition of fayalite (star). A (and A′) represent the composition of a core, B (and B′) represent the composition of the adjacent rim. Composition C in Figure 7N is the outermost part of the rim described by composition B.

in fact be laihunite, *i.e.*, Fe^{3+}-rich fayalite. Mössbauer studies (*e.g.*, Schaefer 1983) will be necessary to evaluate the extent of the laihunite component.

Clinopyroxene

Zoning is found to be most extensive in the granite porphyry. In terms of the cations Ca, Mg and Fe (total iron + Mn) in the clinopyroxene, expressed in atom %, each lithology can be seen to define a distinctly linear trend (Fig. 7). One trend illustrates the crystallization history of the cognate enclaves (M, Fig. 7) and of the two variants of quartz porphyry (N and O, Fig. 7). The trend in the granite porphyry from the ring-dyke (P, Fig. 7) seems slightly displaced in slope. Note that in O and P, the points near the Hd – Fs sideline apparently are deflected toward the Fs corner. This is an artifact of projection only, as here the clinopyroxene composition moves off the plane Wo – En – Fs toward Ac (Fig. 8).

Clinopyroxene in the enclaves (X, Fig. 8) shows a consistently low proportion of the acmite component throughout its crystallization history. The samples of quartz porphyry (Y, Fig. 8) show the same feature until the final stage of crystallization (*e.g.*, in T115, the most evolved sample, according to the composition of fayalite), at which the clinopyroxene rim shows significant enrichment in the acmite component. This very late-stage appearance of a peralkaline phase is attributed to the development of an interstitial Na-rich alkaline fluid phase that reacted with an already formed primary clinopyroxene. In a similar situation, Barker & Hodges (1977) proposed that growth occurred *via* a fluid medium because they could show texturally that the most sodic compositions crystallized after the feldspar and nepheline in undersaturated syenites from the Trans-Pecos province in Texas. At Tibchi, the buildup of Na seems to have occurred once the pyroxene grain was well formed and could fracture (Figs. 3A, B).

The case of the granite porphyry specimens (Z, Fig. 8) is different in a subtle way. The trend labeled AC indicates that the pyroxenes here began to fractionate in conditions identical to those in the quartz porphyry. Significantly, the zonation core C → rim D indicates that the late enrichment in Na and Fe^{3+} took place, as in the samples of quartz porphyry. In addition, however, there are points that lie above the line AC, the most extreme being B, that have a less extreme degree of Fe enrichment than C but that are richer in Na. These points can be regarded as results of attempted re-equilibration of the earlier formed clinopyroxene compositions with the residual peralkaline fluid phase. We infer that this residual fluid remained in contact with the primary crystals for a longer time than in the samples of quartz porphyry, and thus could begin to interact with somewhat more magnesian material located in the core region of the primary crystals.

Note that the pyroxene trends that characterize the enclaves, the quartz porphyry and the granite porphyry share a common initial ferroaugite composition (Fig. 8). This provides another indication of the consanguinity of these lithologies.

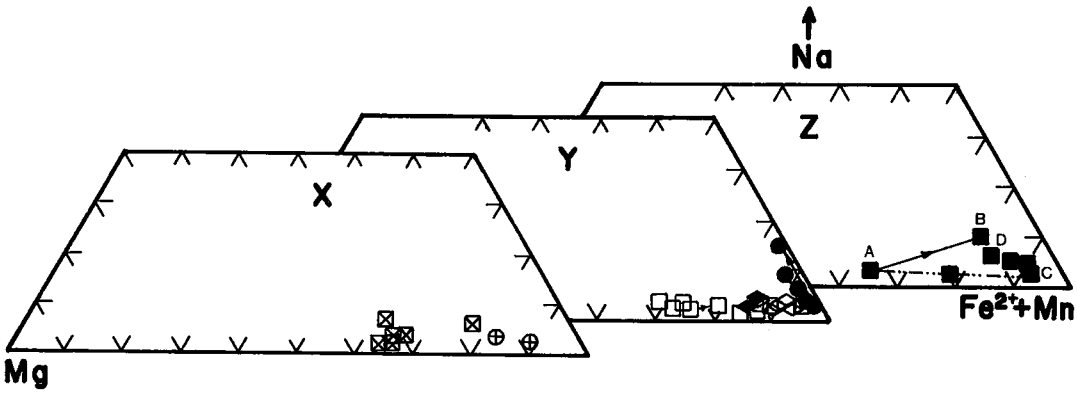

FIG. 8. Plot of the composition of the clinopyroxene in the Tibchi porphyries and related enclaves in terms of atom proportions Mg, (Fe^{2+} + Mn) and Na. Mg represents the diopside end-member, (Fe^{2+} + Mn) represents the hedenbergite end-member, and Na represents acmite. The compositions recorded are grouped according to host rock: X enclaves in the samples of porphyry, Y clinopyroxene in quartz porphyry, Z clinopyroxene in granite porphyry. Tie-lines join zoned crystals, with arrows pointing to the rim. In Z, trend AC, parallel to the base, is considered magmatic in origin; points above the line AC represent clinopyroxene compositions modified at the subsolidus stage by reaction with a circulating aqueous fluid phase.

Discussion

The extreme degree of iron enrichment attained in the evolved rocks of the Tibchi complex invites a comparison with other high-level SiO_2-oversaturated complexes in which differentiation by various processes reached a similar stage. In terms of the clinopyroxene compositions in a diagram Fe – Mg – Na, the Skaergaard trend can be described as a straight line along the base Mg – Fe without sign of late enrichment in Na. However, the extent of Na-enrichment at Tibchi falls short of that seen in more strongly peralkaline complexes, *e.g.*, at Pantelleria (Nicholls & Carmichael 1969) and Nandewar (Abbott 1969). Also, the swing toward acmite occurs at a less strongly Fe-enriched composition in these two complexes; in contrast, the trend toward acmite at Tibchi occurs only after the clinopyroxene composition has virtually reached the Hd – Fs sideline.

The absence of inverted ferriferous β-wollastonite indicates that the Tibchi hedenbergite, $(Ca_{0.862}Mg_{0.008}Fe_{1.130})Si_2O_6$, crystallized directly from a magma, at a temperature below 950°C, according to the experimental data of Yoder *et al.* (1963) and Lindsley *et al.* (1969). In terms of the phase relationships for the join Hd – Fs at pressures up to 2 kbar (Lindsley & Munoz 1969), and considering the most evolved primary clinopyroxene to have a magnesium-free composition, we infer a temperature of crystallization of approximately 800°C. This can also be considered as the upper limit of the temperature at which clinopyroxene – fluid interaction began, though reference to a simple two-component system may well be an unrealistic oversimplification.

In such an extremely iron-enriched system, for example, it is also essential to consider oxygen fugacity as an additonal variable. At the stage of primary crystallization at Tibchi, during which the trend of pyroxene crystallization occurs at constant Ac content, the fugacity of oxygen is presumably buffered at a low level by the assemblage of quartz, fayalite, hedenbergite and ilmenite that coexisted with the water-undersaturated granitic melt. This relatively low fugacity of oxygen may prevent the buildup of the acmite component in the clinopyroxene as magmatic crystallization proceeds. Buildup of Na and Fe^{3+} may begin when the fugacity of oxygen begins to increase, possibly by net loss of hydrogen from the system once a free fluid phase is exsolved during the final stages of crystallization of the interstitial melt. In the absence of coexisting magnetite – ilmenite pairs, this hypothesis cannot be tested at this time.

The emplacement of the quartz porphyry unit by the entrainment of vesiculated and vesiculating magma in a gaseous medium (Ike 1983) implies that a volatile phase did play a key role during, as well as immediately following, emplacement. In rocks of this unit, the fluid phase may have been more plentiful than in the granite porphyry, but in view of limited reactions among minerals, residence time is considered to have been very brief. The quartz porphyry froze in the main conduit that fed the crystal-rich ignimbrites. As a result, the grains of clinopyroxene are only slightly zoned toward acmite at their outermost edge, and there is little evidence of breakdown of fayalite. In contrast, the emplacement of the granite porphyry in the ring-dyke fracture, which followed the fluidization event, involved a relatively quiescent rise of magma, and a crystallization period that allowed the residual fluid to be retained. Although perhaps less plentiful, the peralkaline pore fluid that eventually appeared upon complete crystallization of the granite porphyry probably had a longer residence time, leading to more important interaction with the early-formed clinopyroxene and buildup in the acmite component. The longer time also enabled breakdown reactions to consume fayalite in the granite porphyry at a subsolidus stage; the same reason can be invoked to explain the strikingly more evolved compositions and structures of the feldspars in the granite porphyry (Ike & Martin, in prep.).

Acknowledgements

The senior author expresses his sincere thanks to the Commonwealth Scholarship Commission, London, for financial assistance, and to Ahmadu Bello University, Zaria, Nigeria, for granting a study fellowship. P. Bowden acknowledges the award of grant R2679 from the Overseas Development Ministry, London. R.F. Martin acknowledges the continuing support of the Natural Sciences and Engineering Research Council of Canada (grant A7721), which covered travel to and field expenses in Nigeria. We acknowledge the helpful comments of Drs. A.C. Turnock, D.S. Barker and D. Smith, which led to an improved manuscript.

References

Abbott, M.J. (1969): Petrology of the Nandewar volcano, N.S.W., Australia. *Contr. Mineral. Petrology* **20**, 115-134.

Bain, A.D.N. (1934): The younger intrusive rocks of the Kudaru Hills, Nigeria. *J. Geol. Soc. London* **90**, 201-239.

Barker, D.S. & Hodges, F.N. (1977): Mineralogy of intrusions in the Diablo Plateau, northern Trans-Pecos magmatic province, Texas and New Mexico. *Geol. Soc. Amer. Bull.* **88**, 1428-1436.

BORLEY, G.D. (1963): *Geochemistry of the Mafic Minerals in some Younger Granites of Nigeria.* Ph.D. thesis, Univ. London, London.

BOWDEN, P. (1982): Magmatic evolution and mineralization in the Nigerian Younger Granite province. *In* Mineralization Associated with Acid Magmatism (A. M. Evans, ed.). J. Wiley & Sons, London.

_____ & TURNER, D.C. (1974): Peralkaline and associated ring complexes in the Niger – Nigeria province, west Africa. *In* The Alkaline Rocks (H. Sorensen, ed.). J. Wiley & Sons, London.

BUCHANAN, M.S., MACLEOD, W.N. & TURNER, D.C. (1971): The geology of the Jos Plateau. 2. Younger Granite complexes. *Geol. Surv. Nigeria Bull.* **32.**

FINGER, L.W. (1972): The uncertainty in the calculated ferric iron content of a microprobe analysis. *Carnegie Inst. Wash. Year Book* **71,** 600-603.

IKE, E.C. (1983): The structural evolution of the Tibchi ring-complex: a case study for the Nigerian Younger Granite province. *J. Geol. Soc. London* **140,** 781-788.

_____ & BOWDEN, P. (in press): Electron-microprobe investigation of iron-titanium oxide minerals from the Tibchi complex, Bauchi State, Nigeria. *Nigerian J. Mining Geosci.* **19.**

JACOBSON, R.R.E., MACLEOD, W.N. & BLACK, R. (1958): Ring-complexes in the Younger Granite province of northern Nigeria. *Geol. Soc. London, Mem.* **1.**

LINDSLEY, D.H., BOWN, G.M. & MUIR, I.D. (1969): Conditions of the ferrowollastonite-ferrohedenbergite inversion in the Skaergaard intrusion, east Greenland. *Mineral Soc. Amer., Spec. Pap.* **2,** 193-201.

_____ & MUNOZ, J.L. (1969): Subsolidus relations along the join hedenbergite – ferrosilite. *Amer. J. Sci.* **267A,** 295-324.

MARTIN, R.F. & BOWDEN, P. (1981): Peraluminous granites produced by rock — fluid interaction in the Ririwai nonorogenic ring-complex, Nigeria: mineralogical evidence. *Can. Mineral.* **19,** 65-82.

NICHOLLS, J. & CARMICHAEL, I.S.E. (1969): Peralkaline acid liquids: a petrological study. *Contr. Mineral. Petrology* **20,** 268-294.

SCHAEFER, M.W. (1983): Measurements of iron (III)-rich fayalites. *Nature* **303,** 325-327.

SWEATMAN, T.R. & LONG, J.V.P. (1969): Quantitative electron-probe microanalysis of rock-forming minerals. *J. Petrology* **10,** 332-379.

TURNER, D.C. (1976): Structure and petrology of the Younger Granite ring complexes. *In* Geology of Nigeria (C.A. Kogbe, ed.). Elizabethan Publ. Co., Lagos, Nigeria.

_____ & BOWDEN, P. (1979): The Ningi-Burra complex, Nigeria: dissected calderas and migratory magmatic centres. *J. Geol. Soc. London* **136,** 105-119.

YODER, H.S., JR., TILLEY, C.E. & SCHAIRER, J.F. (1963): Pyroxenes and associated minerals in the crust and mantle. *Carnegie Inst. Wash. Year Book* **62,** 84-95.

Received May 27, 1983, revised manuscript accepted November 14, 1983.